Chapter 2

The experimental setup: design and development

This chapter describes the experimental setup with a focus on new developments realized in the scope of this thesis. Existing and commercial components are described briefly, whereas the new developments, namely a UHV chamber for gas and liquid environment and the generation of tunable sub-20 fs pulses at 100 kHz, are discussed in detail.

2.1 UHV chamber for gas and liquid environment

2.1.1 Motivation

Although the investigation of adsorbates on surfaces is a vividly growing field in science and technology, the fabrication of such interfaces is often limited by technological or system-inherent constraints. Up to now the investigated systems can be divided into two classes: relatively small adsorbates, ranging from atoms to small molecules, on microscopic defined single crystal surfaces and adsorbates (of any complexity) on nano-structured solids. This classification originates from different approaches to this kind of heterogeneous interface, namely surface science in the first case and electrochemistry and photochemistry in the latter. The surface science approach starts from defined single crystal surfaces, which can be prepared by UHV cleaning techniques, e.g. cycles of sputtering and annealing, or appropriate growth techniques like molecular beam epitaxy (MBE). Having a defined sample under UHV conditions, the standard surface science technique for the deposition of adsorbates on a defined surface is the adsorption from the gas phase. Naturally, this method is limited to molecules, which can be brought into the gas phase. However, there is the general trend that the vapor pressure decreases with an increasing size

of the molecule, e.g. the perylene derivatives investigated in this work decompose more efficiently rather than evaporate. This is a general behavior for large molecules exhibiting functionalized units.

To the best of my knowledge, until now only the group of Hans Siegbahn, Uppsala University, Sweden, has published an experimental setup allowing wet chemistry or electrochemistry treatments with the option of transferring the sample from and back to UHV [97, 98]. Their setup is designed as a pure preparation device and is coupled to a setup for photoelectron spectroscopy. The sample subsequently can be dipped in two vessels, one containing a preparation solution, e.g. an electrolyte, and the other a solution for rinsing.

The chamber developed in the framework of this thesis is designed to be used for two different tasks: first, for measurements with the option to switch between UHV, gas and liquid environment, and secondly for wet chemistry preparation at a purity level limited only by the quality of the chemical ingredients.

2.1.2 Description of the chamber

A schematic drawing of the UHV chamber for gas and liquid environment is given in Fig. 2.1. The chamber consists of four units: the main chamber (1), a solvent chamber (2), a pump chamber (3), and a load lock (4). The solvent chamber and the load lock are coupled to the main chamber via CF-35 valves, the pump chamber and the main chamber are connected via a CF-100 valve. The main chamber is equipped with a manipulator (13) with four degrees of freedom allowing the transfer of a sample from the load lock to a position in the optical path (9). A cuvette (Suprasil 1, glass thickness 1 mm) can be moved around the sample at this position via a linear transfer unit. When operating in UHV the main chamber is pumped via the pump chamber, which is equipped with a CF-100 turbo pump and a cold cathode pressure gage. After bakeout the base pressure in the main chamber is in the range 10^{-9} to 10^{-10} mbar. This chamber is equipped with different UHV windows for the application of spectroscopic techniques: two viewports (14) are for pump-probe-spectroscopy in transmission. As entrance window either a commercial fused silica (FS) viewport or a thin home-build UHV compatible window are used. The design of the latter will be described in section 2.1.3. Additionally, a third low-strain FS window (Bomco Inc., not indicated in Fig. 2.1) is provided for the application of reflection anisotropy spectroscopy (RAS) [99].

In the following, the features of the chamber are described together with the handling of the setup.

Inserting the sample: Samples can be brought into the chamber either from lab

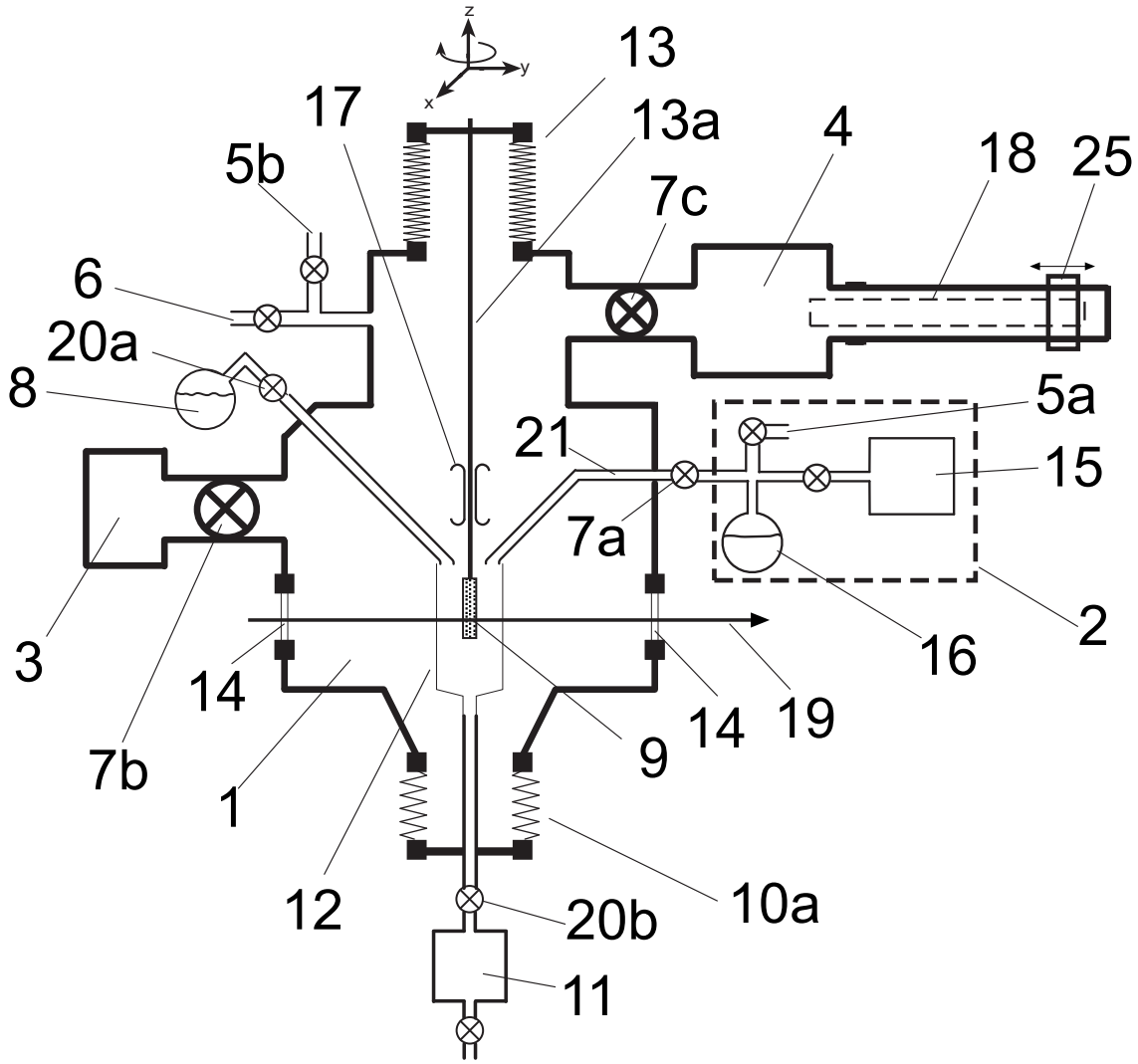

Figure 2.1: Sketch of the UHV chamber for gas and liquid environment. The setup consists of 4 separable units: main chamber (1), solvent chamber (2), pump chamber (3) and load lock (4). Further indicated components are: gas inlet (5a, 5b), gas outlet (6), valves (7a-7c), solvent transport unit (8), sample holder and sample (9), linear transfer unit (10a), liquid outlet with catchment tank (11), cuvette (12), manipulator (13) with rod (13a), UHV viewport (14), turbo pump (15), solvent reservoir (16), sample magazine (17), transfer unit (18) with magnetic slide (25), optical path (19), valve (20a, 20b) and solvent supply (21).

ambient or from a mobile UHV chamber. In the first case, the sample is mounted on a sample holder, which is fixed on a transfer rod (CF-35). The transfer rod is flanged to the load lock, a chamber of small volume equipped with a CF-63 turbo pump and a cold cathode pressure gage. After evacuating the load lock to a sufficient pressure range (10^{-7}-10^{-8} mbar), the sample is transferred into the main chamber. Optionally, samples may be transferred from a mobile UHV chamber, which allows the contamination-free transport of samples between different UHV chambers (or a MOCVD reactor) available in the group [100].

Filling with gas: The main chamber can be flooded with Ar and N_2 via the gas inlet (5b). The gas is provided from bottles (grade 5.0) and streams through electropolished high-grade steel tubes that can be baked out at up to 300 °C at the pressure level provided by a separate turbo pump unit. Optionally, the gas can be conducted through a double stage point-of-use purifier (Oxisorb, Messer Griesheim). There is no limitation in applying more advanced gas purification techniques, if necessary. To control the gas pressure, the chamber is equipped with a UHV compatible piezo-gage suitable for the range 0.1 - 1100 mbar. When filled with gas, the main chamber is separated from the pump chamber. This allows the continuous operation of the turbo pump, which is of advantage for a fast re-evacuation. To remove the gas the main chamber is first evacuated with a rotary vane pump to a pressure below 1 mbar and further with the turbo pump of the pump chamber.

Filling of the main chamber with liquid: The cuvette (12) in the main chamber (volume $\approx$ 50 ml) can be filled with liquids via two independent ways: from the solvent chamber (2), shown in more detail in Fig. 2.2, and from the solvent transport unit (8), which is also included in Fig. 2.2. The availability of two sources in parallel allows a relatively fast exchange of the liquid in the cuvette. From both sources the liquid is brought into the main chamber by the same method, namely simple soaking by generation of a pressure difference. The handling may be explained by considering the solvent chamber (Fig. 2.2). This chamber is connected to the main chamber via a CF-35 slide valve (7a, VAT). There are two tubes on both sides of this valve, one (21) ranging into the cuvette in the main chamber, the other (22) ranging to the bottom of a solvent reservoir (16). The outer diameter of tube (22) is smaller than the inner of tube (21). With opened valve (7a), the whole solvent chamber can be moved by the linear transfer unit (10b) such that tube (22) sticks in tube (21). If the pressure in the main chamber is now lowered compared to the pressure in the solvent reservoir (16), the liquid is soaked through the tubes into the cuvette. The pressure difference can be realized, as the solvent chamber is divided into two volumes, a anteroom (26) and a main room (29). These two volumes are connected via tube (22) and valve (20c). With valve (7a) being open, the pressure in the anteroom (26) equilibrates with the main chamber. Thus, closing valve (20c) allows the generation

of a pressure difference, which tends to equilibrate via tube (22), and thereby soaks in the liquid. The liquid flow can be stopped rather abruptly by simply opening valve (20c).

The filling of the cuvette from the solvent transport unit (8) is done similarly. The transport unit is shown in Fig. 2.2 (dashed box), as it is also used for filling the solvent chamber. The transport unit is a round-bottomed flask with a glass-metal transition and a CF-16 closure. The closing flange exhibits lead-throughs for two tubes, one ranging to the bottom of the flask. The tubes are closed with valves. The transport unit is connected via a branch connection (30) and a valve (20a) to a tube ending in the cuvette. After the connection is established ambient air and water in the branch connection is removed by evacuation via the third port and parallel heating of the branch connection. The liquid can then be soaked into the main chamber again by applying a pressure difference.

This soak-in method has been applied for different reasons:

- The liquids are only in contact with the inlet tubes.
- The method can be realized by use of high-grade steel UHV components.
- It seems plausible that the impurity concentration in a static liquid is higher at the surface, compared to the liquid bulk, especially of those impurities with opposite polarity than the liquid itself. As the liquid is soaked from the bottom of the reservoirs, the surface layer of the liquids does not enter the main chamber. Furthermore, as the sample can already be positioned inside the cuvette while the latter is filled, the sample is dipped in a practically non-static liquid and does not have to cross a smooth liquid surface.

The liquid is removed from the chamber via the liquid outlet connected with an evacuable catchment tank (11), again by simple soaking of the liquid. Optionally, the liquid can be blown out of the cuvette by increasing the pressure in the chamber above atmosphere pressure in the lab, if the catchment tank is not mounted.

Solvent purification in the solvent chamber: The main difference between filling the cuvette from the transport unit (8) or from the solvent chamber (2) is that the latter provides the option for a solvent purification procedure, namely freeze/pump/thaw cycles (or "pump-and-freeze"). This method reduces the amount of dissolved oxygen in a liquid. Therefor the liquid is frozen within the solvent reservoir (16) by surrounding the flask with liquid N_2 in a Dewar vessel. Once the solvent is frozen, valve (7d) is opened and the volume is evacuated with a turbo pump (15). Then valve (7d) is closed and the liquid thawed by surrounding the flask (16) with a water bath. During the melting, the volume might be filled via the

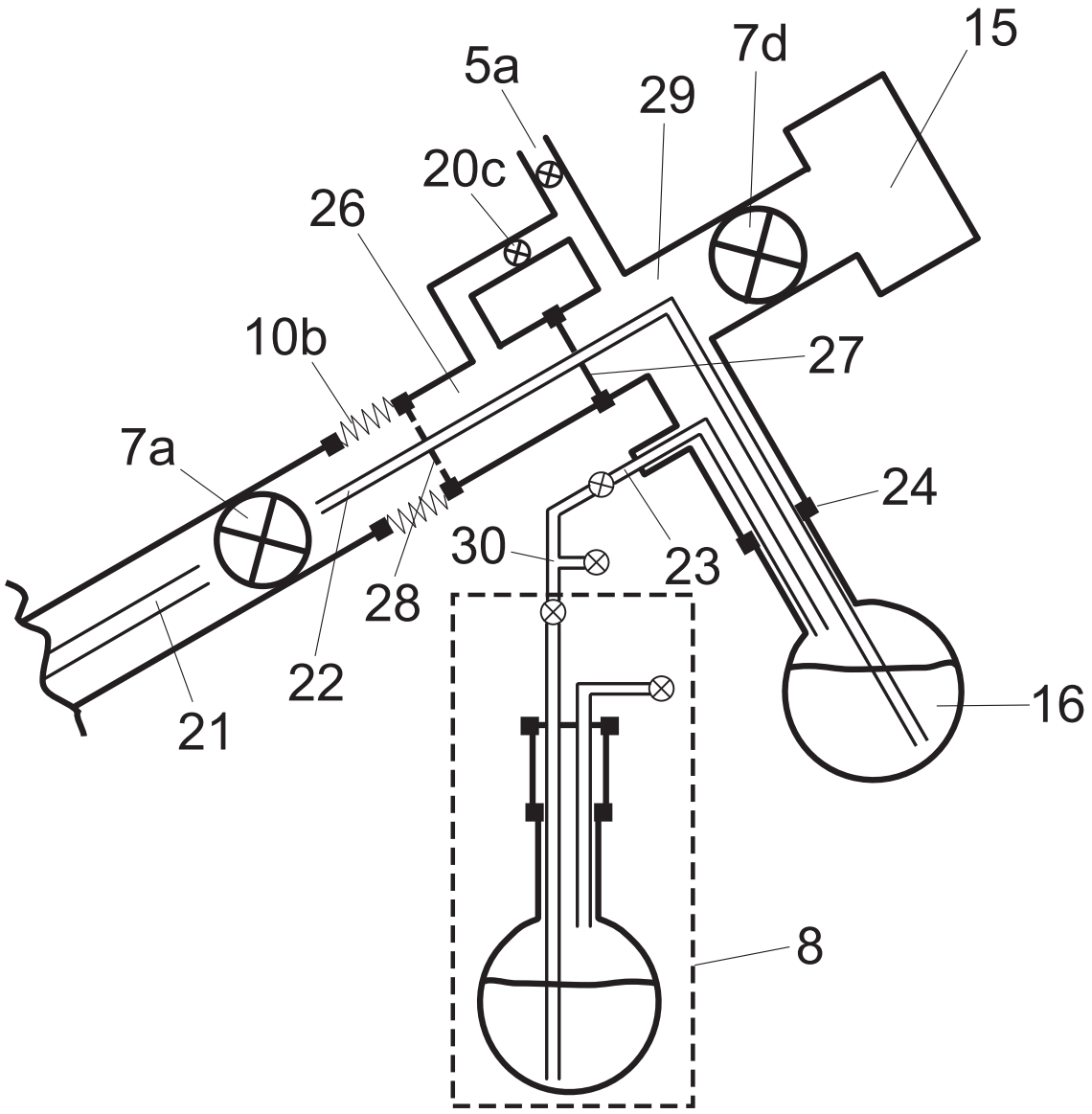

Figure 2.2: Details of the solvent chamber (2): gas inlet with valve (5a), valves (7a, 7d), turbo pump (15), solvent reservoir (16), tube (21) ranging in the cuvette of the main chamber, tube (22), liquid inlet with valve (23), metal-glass transition (24), anteroom (26), vacuum sealed lead-through (27), open lead-through (28) and main room (29). Additionally, the solvent transport unit (8) is drawn, connected via a branch connection (30).

gas inlet (5a) with inert gas (Ar, N_2), provided from the same source as used for the main chamber. The liquid might then be refrozen and the procedure repeated.

Filling of the solvent chamber and the transport unit: The solvent chamber can be filled via two different ways as well. First by use of the transport unit, as indicated in Fig. 2.2. The procedure is identical to the filling of the main chamber with the transport unit. Secondly, by use of a mobile distillation setup, consisting of a flask containing the liquid and metallic sodium, and a water cooled condensation unit connected to the liquid inlet (23). The removal of water and oxygen from liquids by metallic sodium is a standard technique in chemistry. It should be noted that this method can be applied to pure solvents but usually not to dye solutions.

The transport unit is filled from a distillation setup installed in a chemistry lab. Again, the liquid is evaporated out of a mixture with metallic sodium. The volume between the distillation setup and the transport unit as well as the transport unit itself are evacuated and refilled with inert gas several times before filling it with solvent. A dye solution can be produced in the transport unit by giving a weighted amount of solid dye beforehand and proceeding as above.

For particular applications an electrochemical treatment of the surface might be interesting. There is no technical constraint to equip the main chamber with electrodes ranging into the cuvette (12). Filling the cuvette with an electrolyte would then allow such a electrochemical manipulation.

The device described above as well as the method of the high-purity wet chemistry preparation have been applied for patent at the Deutsches Patent- und Markenamt.

2.1.3 Construction of a thin UHV window

Short light pulses are altered in their temporal profile by the propagation through dispersive media like the window of a UHV chamber. To the best of my knowledge, the thinnest commercially available UHV viewports have a thickness of 1 mm (Vacom), the standard thickness is about 3 mm. For pulses with finite bandwidth, the linear temporal chirp introduced by the window material can be easily precompensated with standard pulse compression schemes like a prism compressor. Nevertheless, the reduction of the dispersion in the optical path is of advantage, because the compensation of higher order chirp, which becomes more significant with increasing bandwidth and increasing center frequency of the pulse, requires more laborious methods. Furthermore, the application of unamplified white-light continua (wlc, also called "supercontinuum") as probe pulses is an attractive spectroscopic technique [101, 102]. Usually this supercontinuum probe pulses are applied without pulse shaping [40, 21]. Therefore the achievable time resolution depends mainly

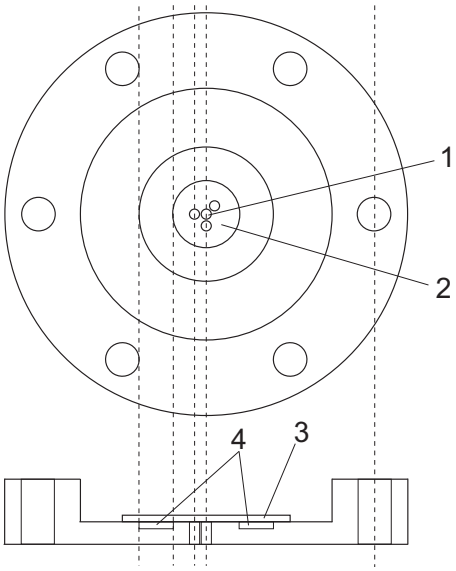

Figure 2.3: Thin UHV window: aperture (1), bearing area (2), window material (3) and glue channel (4).

on the linear temporal chirp acquired by the wlc between generation and sample. For the application of supercontinuum probe pulses in a UHV chamber, the dispersion induced by a commercial viewport is the limiting factor regarding the time resolution.

Fig. 2.3 shows the scheme of a UHV window with a window material of 140 μm thickness [103]. The window is fabricated from a standard blank flange, a microscope cover slip (Menzel, glass type D263 T) and UHV compatible 2-components silver glue. The fabrication is cheap and simple. The blank flange is thinned to about 2 mm thickness and several apertures (diameter: 2 mm, center-to-center distance: 2.5 mm) are drilled around the center to allow different geometries for the pump and probe beams. As the distance between window and sample is about 10 cm, pump and probe beams propagate with an angle of 1.4° through the sample. Around the center bearing area a channel is milled as receptor for the glue. The window shows good long-term stability. The use of different window material, e.g. fussed silica for UV pulses, is possible.

A supercontinuum is generated from a pulse centered at 800 nm with a typical energy of 500 nJ. Most of the energy of the supercontinuum pulse remains in the spectral range of the generating pulse. For comparison: the energy of the pump pulses is typically 10 - 50 nJ. If the visible range is of spectroscopic interest the high intensity around 800 nm passes the sample prior to the detected wavelength due to the up-chirp of the wlc. That might introduce artifacts, especially for the situation of temporal overlap of pump pulse and intensity maximum of the supercontinuum probe. Hence the wlc has to be smoothed or the spectral region around the gen-

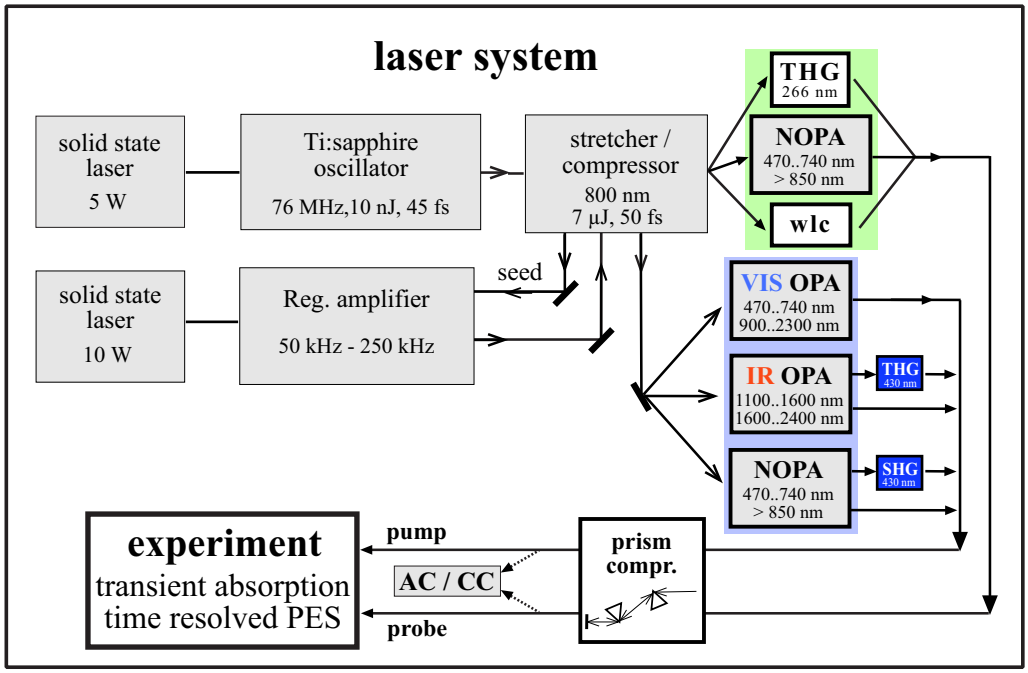

Figure 2.4: Scheme of the laser system. Different nonlinear optical conversion schemes allow for the generation of tunable pump and probe pulses. The options in the generation of the pump and the probe pulses are indicated within the blue and the green box, respectively.

erating pulse has to be filtered prior the sample. Therefore, the window material has been coated with a dielectric coating that is high-reflective (HR) for the spectral region 720 - 880 nm and transparent below and above that range. The coating (Layertec) has be designed such that the group velocity dispersion introduced to the pulse in transmission is a smooth function throughout the visible. The spectral region around the fundamental wavelength can thus be removed from the wlc without introducing additional dispersion in the optical path.
This design of a UHV window has been applied for patent as well.

2.2 Laser system

2.2.1 Overview

Laser pulses for the transient absorption measurements were generated with a commercial 50-250 kHz repetition rate Ti:Sapphire fs-laser system (Coherent Instruments, seed: Mira 900, amplifier: RegA 9050) operating at 800 nm. A scheme of the laser system is given in Fig. 2.4. The pump sources of both oscillator and amplifier were subsequently changed in the course of this work. Starting with a single Ar^+-laser (Coherent Sabre) pumping both oscillator and amplifier, the Ar^+-laser

was first replaced by solid state lasers for the amplifier and then for the oscillator (Coherent Verdi 10 W and Verdi 5 W, respectively). The laser system provides pulses of 6 μJ energy and 50 fs pulse duration full width half maximum (FWHM).

The laser system is used for different spectroscopic techniques (transient absorption and pump-probe photoelectron spectroscopy [104]) on different systems, which requires different pump and probe wavelengths. For the perylene system studied in this thesis, pump pulses in the spectral range of 425-450 nm are necessary. This spectral region is hard to access with a Ti:Sapphire laser system operating around 800 nm as it is above the frequency-doubled of the fundamental wavelength [105] and below the range achievable with a single conversion step. This requires a detour via the infrared (IR). Initially, the pump pulses were generated by frequency-tripling the IR output of a commercial IR optical parametric amplifier (Coherent) [106]. This scheme provides easily tunable blue output with sufficient pulse energy, but with limited bandwidth of about 500 cm^{-1}.
To achieve more bandwidth and thus shorter pump pulses, other conversion schemes have been tried. The spectral broadening of the 800 nm fundamental by self-phase modulation in a sapphire plate, a single mode fused silica fiber, or a photonic crystal fiber and the subsequent frequency-doubling did not succeed: The sapphire attempt resulted in broad blue spectra with acceptable pulse energy, but with poor stability with respect to spectrum and energy. The approach with the fibers failed due to the limited energy throughput of the fibers.
The succeeding approach, the adaptation of the NOPA scheme to the high repetition rate laser system, resulted from a collaboration of the group of Prof. E. Riedle, in particular J. Piel and E. Riedle, LMU Munich, and the laser group at the HMI.

This NOPA is interesting for many spectroscopic applications in physics, chemistry and biology, as widely tunable laser pulses with a duration of less than 20 fs are needed to resolve the ultrafast dynamics on the time scale of nuclear motions within the constituents. But many samples are seriously damaged when absorbing strong laser pulses. Therefore measurements with weak laser pulses and thus high repetition rate are required to achieve sufficient signal-to-noise ratio.
The principle of non-collinear amplification was proposed in 1995 [26] and realized by the groups of Riedle [27] and Silvestri [107] in 1997. For laser systems in the one kHz range, which provide pulses of hundreds of μJ. This conversion scheme is now well established [108].
The other limit with respect to the repetition rate is the oscillator frequency. Limited tunable sub-20 fs pulses are obtainable from optical parametric oscillators at 80 MHz [109]. However, for many spectroscopic applications this repetition rate is too high, as it does not allow the investigated system to fully recover or to be exchanged within the pulse separation of 12.5 ns.

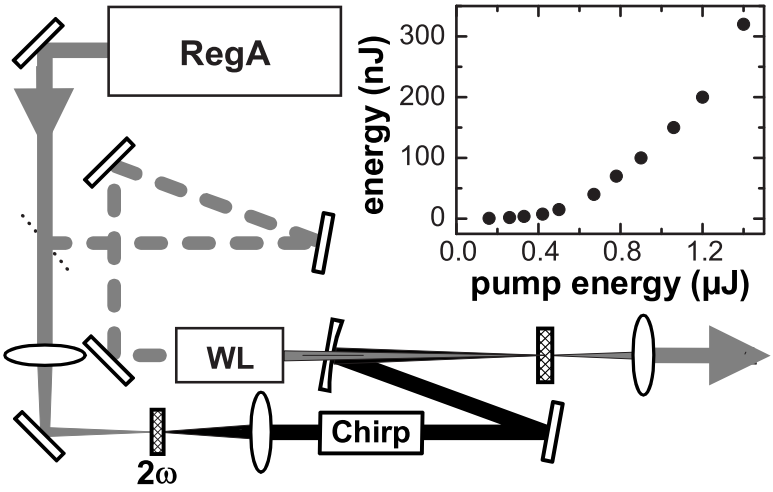

Figure 2.5: Scheme of the single stage NOPA. 10% of the 800 nm input is used to generate a single filament white-light (WL) continuum as seed. The remaining of the fundamental is frequency-doubled, temporally streched, and superimposed with the seed in a non-collinear phase-matching geometry. The inset shows the output power at 500 nm in dependence of the pump pulse (400 nm) energy. Figure from Refs. [110, 111].

The intermediate range is therefore of great interest. The following section describes the design and the performance of the 100 kHz NOPA.

2.2.2 100 kHz NOPA

It has been demonstrated that the single stage NOPA can generate sub-20 fs tunable visible pulses with an output pulse energy of up to 750 nJ. This maximal output was achieved with the NOPA pumped with the full 7 μJ pulse energy available at 800 nm (after the compressor). This pulse length is significantly shorter and the output energy is considerably higher than previously obtained with a double stage collinear amplifier [112]. The design of the NOPA is shown in Fig. 2.5.
The low energy pump requires a careful optimization of the setup. This was obtained by J. Piel by gradually lowering the pulse energy from a kHz system to the input level available at 100 kHz. The NOPA output at 500 nm obtained in this way is shown as inset in Fig. 2.5 in dependence of the energy of the blue pump pulses for even further lowered pulse energies. It can be seen that scalability can even be obtained at blue pump energies well below 1 μJ, i.e. at red input of 3 μJ or less. The maximal reached blue pump energy with the 100 kHz laser system was 2.7 μJ.

Only 10% of the red pump light is used to generate a single filament continuum in a

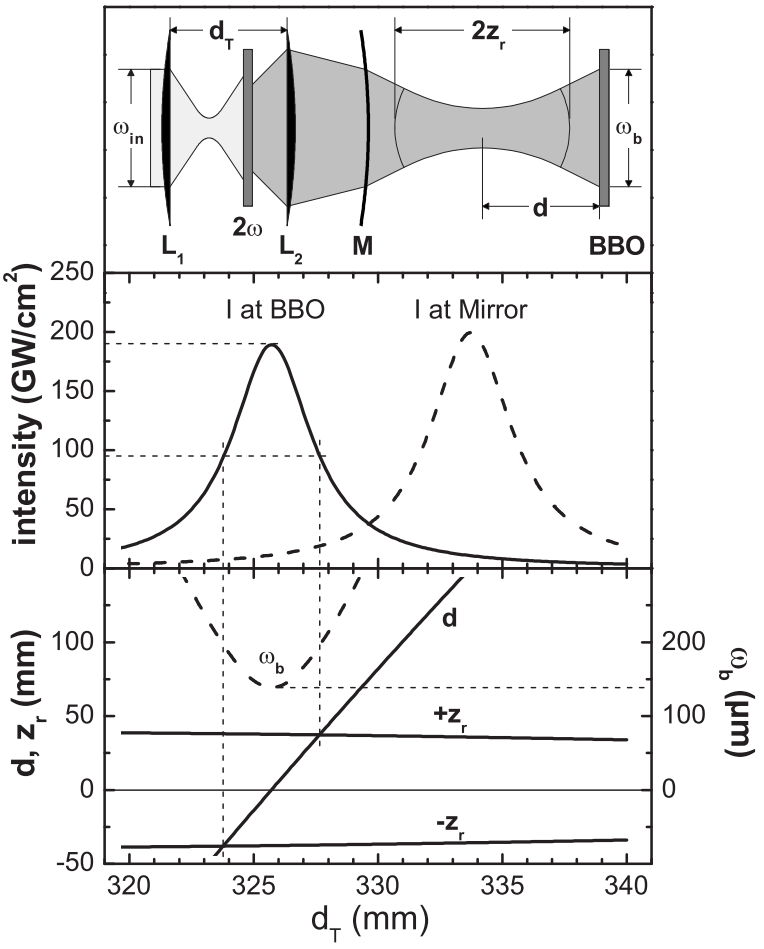

Figure 2.6: Detailed graphic of the beam geometry within the NOPA (upper part). The distance d_T of the focusing lens L_1 and the recollimating and refocusing lens L_2 is the free parameter to adjust the pump intensity to 150 - 200 GW/cm^2. The middle and lower part shows the pump beam waist ω_b, the pump intensity I at the BBO, the Rayleigh range $2z_r$, and the walk-off d of the focus in dependence of d_T. Figure from Refs. [110, 111].

3 mm sapphire plate. The main part of the light is frequency doubled in a 300 μm BBO crystal placed in the focus of lens L_1 or slightly behind (see Fig. 2.6). To ensure a good temporal overlap of the blue light with the chirped seed light a dispersive element consisting of two fused silica plates is inserted. The stretched 400 nm light is used to amplify a broad spectral slice of the continuum seed light in a 2 mm BBO crystal. It has been shown before that an appropriate non-collinear geometry leads to simultaneous phase matching throughout most of the visible and consequently very broadband visible pulses [108]. For the 100 kHz pump system it is best to place the amplifier crystal within the Rayleigh range $2z_r$ of the focused blue light, which is in contrast to the 1 kHz NOPAs. Fig. 2.6 gives a detailed view of the beam geometry. The upper part illustrates the optical path of the pump pulse. Behind the doubling crystal the pump light is recollimated and refocused with the fused silica lens L_2. Behind L_2 the remaining 800 nm light is removed from the pump beam by two mirrors which are highly reflective for 400 nm only. One of these mirrors is mounted on a translation stage, which is used to adjust the temporal overlap of the pump and the seed pulse. The second is a concave mirror M (r = 1 m), which further focuses the pump beam.

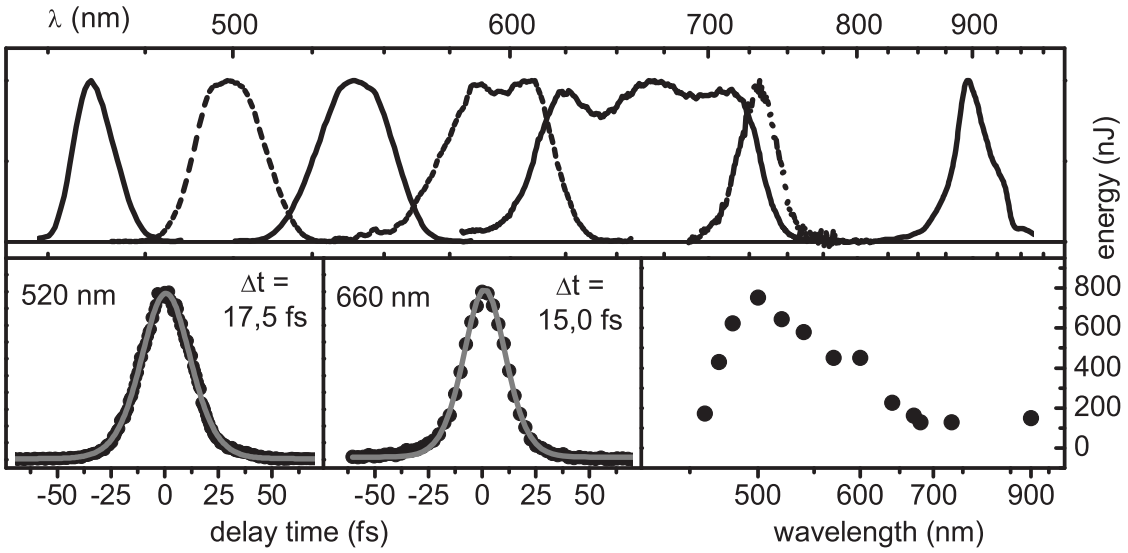

Figure 2.7: Output spectra, exemplary autocorrelation traces and tuning curve for the NOPA. The maximum pulse energy of 750 nJ was obtained with 7 μJ pulses at 800 nm. Figure from Refs. [110, 111].

The variation of the spacing d_T between the lenses L_1 and L_2 allows the adjustment of the beam waist ω_b of the blue pump in the BBO crystal and thus the tuning of the intensity in the amplifier crystal ("I at BBO"). This is illustrated in the middle and the lower part of Fig. 2.6. The intensity was adjusted to about 150 - 200 GW/cm^2. The BBO crystal is mounted on a translation stage to correct for the walk-off d of the focus from the BBO position when d_T is varied. The calculations were performed by J. Piel.

The NOPA is tunable from 460 nm to well beyond 1 μm (for sample spectra see Fig. 2.7) with spatial modes of the output very close to Gaussian fundamentals. The spectral bandwidth is sufficient for sub-20 fs pulses through most of the tuning range. Exemplary the lower part of Fig. 2.7 shows two auto-correlation (AC) traces for pulses around 520 and 660 nm. The pulses were compressed with a standard fused silica prism compressor.
At the maximum of the tuning curve a pulse energy of 750 nJ is obtained corresponding to a quantum efficiency of more than 30% from the blue and an overall energy conversion efficiency (800 nm to green) of about 10%. The efficiency falls off toward longer wavelengths because of signal/pump group velocity mismatch (GVM). The GVM is zero for signal pulses around 490 nm and increases to 150 fs/mm for 700 nm. The effective overlap of a given spectral component with the 400 nm pump pulses decreases correspondingly to only 1 mm of the 2 mm amplifier crystal. The non-collinear phase-matching adjusts only the signal/idler GVM to zero [108].

In conclusion, the single stage NOPA is a simple, compact and stable device that

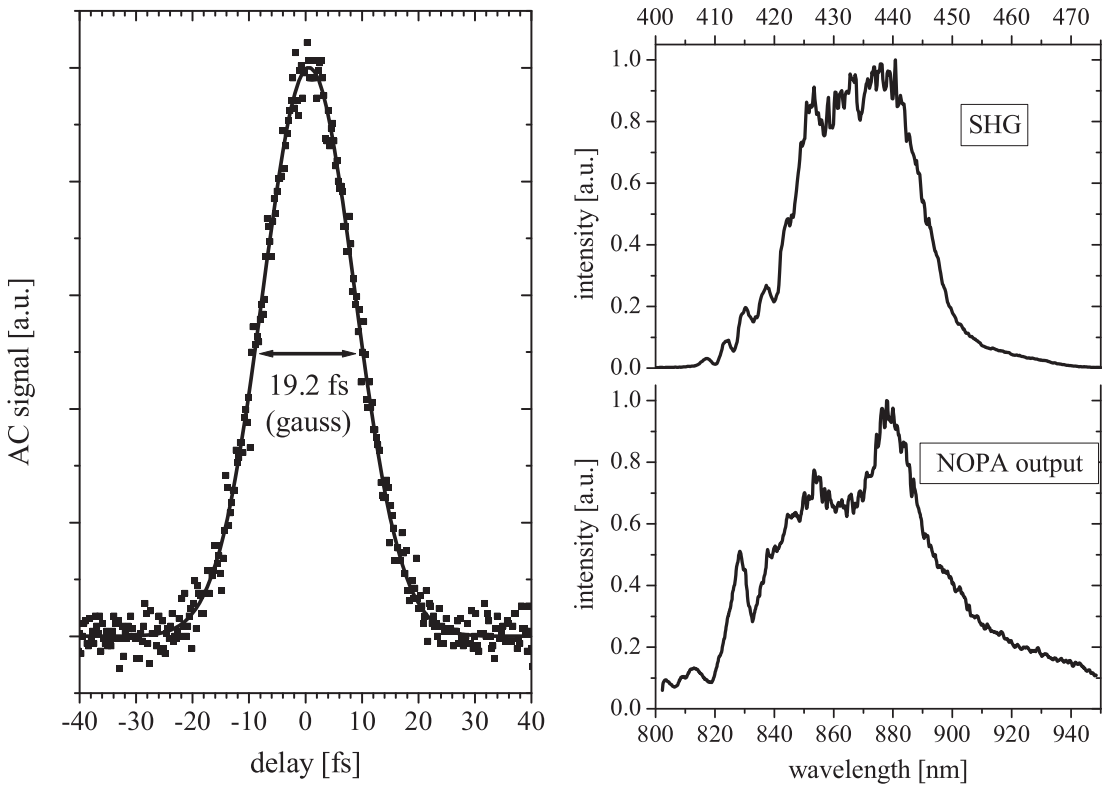

Figure 2.8: Sub-15 fs pump pulse. Left panel: AC trace of a 433 nm pump pulse taken with a SiC diode. The fit with a Gaussian (solid line) indicates a pulse duration of 13.6 fs. The spectrum of the pulse is shown on the right. Right panel: Spectra of the NIR NOPA output behind a RG830 filter (lower part) and the frequency-doubled spectrum (upper part). The pulse energies of the NIR and the blue pulses are in the range of 100-150 nJ and 20-40 nJ, respectively.

generates significantly shorter pulses with additionally higher pulse energy compared to a double stage collinear OPA. A decreased chirp of the seed continuum together with an improved compression scheme should even lead to sub-10 fs pulse durations.

2.2.3 Generation of sub-15 fs pulses around 430 nm

Pump pulses suitable for the excitation of the perylene chromophore are generated by frequency-doubling of the near infrared (NIR) output. The NIR wavelengths are also generated on axis and utilize the NIR part of the seed light [113]. It should be noted that the non-collinear phase-matching condition is not fulfilled in this geometry. Nevertheless, a broad-band amplification can be achieved due to the GVM of blue pump and NIR signal. The right panel of Fig. 2.8 shows the spectra of the NIR NOPA output behind a RG830 filter. The frequency doubled spectrum is shown on top. The second harmonic is generated by tightly focusing the NIR with a microscope objective into a 100 μm BBO crystal. It can be seen that the broad

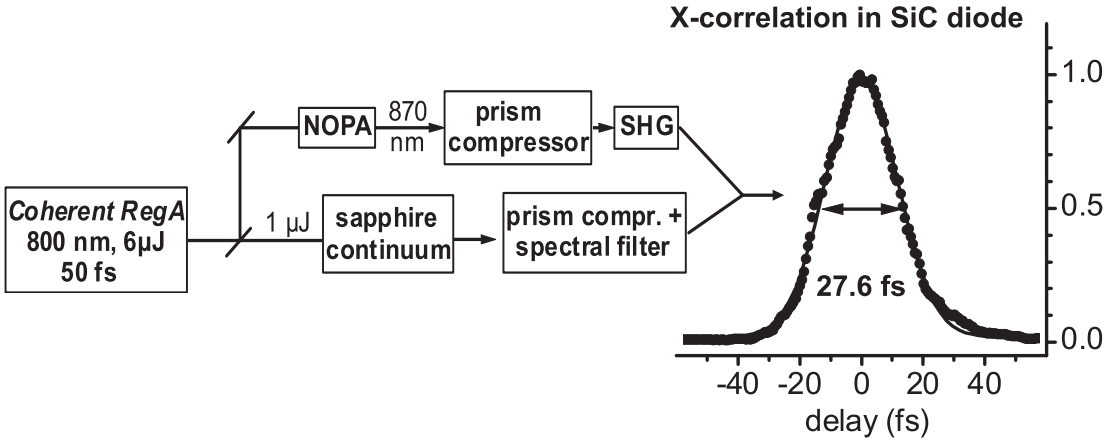

Figure 2.9: Experimental setup of the pump-probe experiment. The system function is below 30 fs.

bandwidth is effectively transferred into the blue. Additionally, the phase-matching condition of the second harmonic generation (SHG) "cleans up" the blue spectrum. The left panel in Fig. 2.8 shows the AC trace of the blue pulse taken with a SiC-diode (see section 2.2.5). The fit with a Gaussian indicates a pulse duration of 13.6 fs. The compression of the blue pulses is realized by down-chirping the NIR pulse, i.e. by a fused silica prism compressor before the SHG (180 cm prism separation).
To the best of my knowledge, this is the first report of sub-20 fs pulses in the spectral range 425-450 nm.

2.2.4 Probe pulses

Probe pulses are obtained by two ways, either by the spectral filtering of pulses from an unamplified white-light continuum or by the use of the output of a second NOPA. For both options, the probe pulse energy is kept below 10% of the pump energy. The achieved pulse durations was very similar for both methods. The way how to operate two NOPAs in parallel will be discussed in detail elsewhere [104]. The pulse generation scheme is summarized in Fig. 2.9.

2.2.5 Autocorrelation (AC)

The characterization of single pulses was achieved by intensity-autocorrelation utilizing 2-photon induced photoconductivity [114] and SHG. The setup was a standard Michelson interferometer with variable non-collinearity of both arms. The delay of one arm was achieved by a spring geared retro reflector with position sensor (APE, Scan Delay 15), driven with a 10 Hz sinosodial function generated by an external function generator (HP 33120A). The scanner has been calibrated by taking the

interferogram of a HeNe-Laser.

The AC signal was recorded either with a 100 kHz 16-bit analog digital converter (ADC) (National Instruments) or with a 1 GS/s 8-bit ADC with on-board averaging (Acqiris AP100, 8 Mpoints on board memory). The latter ADC allows data acquisition at rates more than a factor of 1000 higher than the repetition rate of the laser system, resulting in an effective increase of the ADC resolution and an efficient reduction of high frequency noise (above the laser repetition rate) of the photodiode and its amplifier. This setup provides reliable AC traces with an update frequency of about 1 Hz.

2.2.6 Cross-correlation (CC)

The system function of the transient absorption measurements was mostly determined by 2-photon induced photoconductivity in SiC. The reliability of this method was studied by Lochbrunner, Huppmann and Riedle and found to be superior compared to SHG [115]. To assure oneself, the SiC-CCs have been compared to other signals:

- SHG-CCs with 25, 50 and 100 μm thick BBO crystals. Usage of 100 μm thick BBO crystals (and for large bandwidth pulses also 50 μm crystals) resulted in erroneous CC traces suggesting shorter pulse length due to the insufficient acceptance bandwidth.

- Non-resonant coherent signals taken in a 140 μm glass plate. This method usually is utilized for the characterization of chirped supercontinuum pulses [101]. Due to the low pulse energies, this effect gives rise to approximately 10^{-4} transmission change. Therefore, this method is not very practical.

- Non-resonant coherent signal taken in a 500 μm TiO_2 rutile single crystal. In contrast to glass, rutile shows a strong coherent signal, whereas the pulses strongly broaden [116] and shift in time relative to each other due to the group velocity dispersion (GVD) of rutile. But as the probe pulse propagates faster through the crystal than blue pump pulse, the rising edge of the signal, or rather its derivation, can be used to measure the CC.

SiC-CC, SHG-CC in a sufficient thin crystal, and the coherent signal agree well with each other, whereas the SiC-CC and the rutile method are the most convenient measurements. The SiC diodes (Lasercomponents JEC 0.1S and JEC 0.3S) current is converted to a voltage with a standard operational amplifier (Burr-Brown OPA 111).

CC traces are measured outside the UHV chamber. The dispersion introduced by the UHV window is simulated, i.e. the optical paths correspond except of 10 cm air (instead of vacuum). The CC data is acquired with a Lock-In amplifier while the delay is slowly scanned (500 ms per point).

2.2.7 Data acquisition

The pump and the probe pulses were focused to spot sizes of about 150 and 100 μm, respectively. The probe pulses are delayed with a 30 cm motor stage with 0.1 μm resolution. The beam geometry in the sample is non-collinear with an angle of 1.4°. The polarizations of pump and probe pulses are kept parallel. The pump pulse energy at the sample is between 10 and 30 nJ, the probe pulses energy typically 300 pJ.

The pump-probe signal is taken with Lock-In technique. The pump beam is chopped with a frequency of about 400 Hz and blocked after the sample. The probe beam is spectrally resolved with a monochromator (with a resolution about 2 nm) and detected with a photodiode. The Lock-In data is acquired at about 1 Hz (Lock-In time constant: 100 ms) via GPIB together with the position of the delay line and of the monochromator. The transient absorption data shown in this thesis was averaged over multiple scans (typically 5 to 15). Transmission changes of about 5×10^{-5} are detectable with this number of scans.